metals

MDPI

Article

Study on the Microstructure Evolution of Mg-1Ca-(2Ag) Alloys During Hot Rolling and Its Corrosion Properties

Qingfu Qian [1], Daliang Sun [1,2], Zaijiu Li [1,3,4,*], Qinglin Jin [1] and Yikai Sun [1]

[1] Faculty of Materials Science and Engineering, Kunming University of Science and Technology, Kunming 650093, China
[2] Baoti Group Co., Ltd., Baoji 721017, China
[3] School of Electronic and Information Engineering, Anshun University, Anshun 561000, China
[4] Faculty of Civil Aviation and Aeronautics, Kunming University of Science and Technology, Kunming 650500, China
* Correspondence: lizaijiu@126.com

Abstract

Magnesium alloys' poor corrosion resistance limits their applications as biodegradable bone repair materials. Alloying tailors Mg alloys' microstructure and properties. The present study investigates the effect of 2 wt.% Ag addition on the microstructure and initial corrosion behavior of hot-rolled Mg-1Ca alloy. Mg-1Ca and Mg-1Ca-2Ag alloys were prepared by melting using Mg-2Ca and Mg-4Ag master alloys, followed by homogenization at 400 °C for 2 h, hot rolling, and stress-relief annealing at 400 °C for 6 h. The alloys were systematically characterized using field-emission scanning electron microscopy (FESEM), transmission electron microscopy (TEM), electron backscatter diffraction (EBSD), and X-ray diffraction (XRD). Initial corrosion behavior was evaluated via 3 h immersion tests in simulated body fluid (SBF). Results reveal Ag's high thermal diffusivity promotes segregation at tensile twin boundaries, forming Ag_3Mg nanoparticles. These nanoparticles hinder grain boundary migration and, with increased deformation, facilitate grain rotation and high-angle grain boundary formation, weakening texture. Internal stress accumulation near twin boundaries—driven by grain orientation variation and nanoparticles—induces ~86° rotation of {10–12} tensile twins around the c-axis, forming double twins. During corrosion, nanoparticles and double twins synergistically promote dense protective film formation, significantly reducing corrosion rates.

Keywords: Mg-1Ca-2Ag alloy; Ag addition; Ag_3Mg nanoparticles; double twins; microstructure; corrosion behavior

Check for updates

Academic Editor: Marcello Cabibbo

Received: 22 January 2026
Revised: 10 February 2026
Accepted: 11 February 2026
Published: 13 February 2026

Copyright: © 2026 by the authors. Licensee MDPI, Basel, Switzerland. This article is an open access article distributed under the terms and conditions of the Creative Commons Attribution (CC BY) license.

1. Introduction

As a class of lightweight metallic materials, magnesium (Mg) and its alloys possess a series of advantageous properties, including low material cost, low density, and high specific strength, which render them highly attractive for applications in aerospace engineering [1], electronic devices [2], and biomedical fields [3]. In particular, magnesium-based alloys have recently attracted extensive attention as promising candidates for biodegradable bone implant materials. This interest primarily stems from their unique combination of physical and biological characteristics, such as density and elastic modulus close to those of natural human bone, as well as their ability to undergo gradual degradation in vivo without generating toxic or harmful byproducts [4]. These features enable magnesium alloys to effectively reduce stress shielding effects while eliminating the need for secondary

surgical removal after implantation. Despite these advantages, the practical application of Mg-based alloys in bone tissue engineering is still severely restricted by their intrinsically high electrochemical activity. The large electrochemical potential difference between magnesium and physiological environments often results in excessively rapid corrosion and uncontrolled degradation rates, leading to premature loss of mechanical integrity before sufficient bone regeneration occurs. Consequently, the rapid degradation behavior of magnesium alloys remains one of the most critical bottlenecks limiting their clinical application in biodegradable bone repair. Therefore, enhancing the corrosion resistance of magnesium alloys while maintaining their biodegradability and biocompatibility has become a key research focus in the field of biodegradable metallic materials.

Previous studies have demonstrated that microstructural refinement and controlled precipitation of secondary phases are effective strategies for improving the corrosion resistance of Mg-based alloys. These improvements can be achieved through a combination of microalloying and thermomechanical processing. With respect to microalloying [5–7], the selection of alloying elements must not only improve mechanical and corrosion properties but also strictly comply with biosafety requirements for biodegradable implant materials. To date, alloying elements such as zinc (Zn) [5], calcium (Ca) [6–10], lithium (Li) [11], and silver (Ag) [12–19] have been extensively investigated. Among these elements, Zn, Ca, and Li are characterized by low atomic weight and favorable biological functions, including participation in cellular signaling and bone metabolism [20]. In contrast, Ag is well known for its excellent antibacterial activity, which can be imparted to Mg alloys through the sustained release of Ag^+ ions, thereby effectively inhibiting bacterial adhesion and proliferation on implant surfaces. In addition to alloying strategies, plastic deformation processing plays a crucial role in tailoring the microstructure and corrosion behavior of magnesium alloys [21]. Grain refinement strengthens via Hall–Petch and promotes uniform corrosion by increasing boundary barriers to pitting. Deformation-induced features hinder diffusion, enabling nanoscale precipitates that enhance both mechanics and corrosion. Examples include refined Mg–Zn–Ca via forging [22] and Ag/Li/Zn-alloyed Mg with antibacterial benefits [23]. Ca, abundant in bone, aids biosafety, osteoblast activity, and regeneration [6–10]; combined with Ag's antibacterial action, Mg–Ca–Ag systems show strong orthopedic potential.

The base alloy selected is Mg-1Ca, as ~1 wt.% Ca optimally refines grains, minimizes excessive Mg_2Ca phases (which accelerate corrosion at higher contents), ensures biosafety, and promotes bone regeneration via Ca's role in osteogenesis [6–10], literature consensus on <1–1.3 wt.% Ca optimal. Hot rolling was chosen to achieve uniform refinement, dislocation/twin introduction, and controlled precipitation for balanced properties. Adding 2 wt.% Ag justifies strong antibacterial Ag^+ release, refined precipitates for corrosion/mechanical gains, and biosafety (sufficient without excessive toxicity seen at higher Ag) [12–19], common in Ag-Mg studies for balance. Prior Mg–Ca–Ag work emphasizes mechanics/strengthening [24,25], with limited focus on Ag-driven corrosion mechanisms. This study addresses Ag-induced evolution during hot rolling in Mg-1Ca. Notably, the precipitation of Ag_3Mg nanoparticles at twin boundaries and their promotion of double twin formation in Mg–Ca–Ag remain rarely reported, offering novel insights into microstructural control for enhanced performance in biodegradable bone repair.

2. Materials and Methods

The flowchart of alloy preparation is shown in Figure 1. The Mg-1Ca-2Ag (wt.%) alloy was fabricated by melting Mg-2Ca and Mg-4Ag master alloys in equal mass proportions using a resistance furnace (Carbolite Gero, Neuhausen, Germany) under a protective Ar/SF_6 atmosphere. The melting temperature was set to 800 °C and maintained for 10 min to ensure adequate mixing and chemical homogeneity of the molten alloy. Subsequently, the melt was cast into a preheated steel mold to obtain as-cast ingots. The solidified ingots were then machined into rectangular specimens with dimensions of 25 mm × 15 mm × 50 mm. To minimize elemental segregation and enhance compositional uniformity, the machined specimens were subjected to a homogenization heat treatment at 400 °C for 2 h prior to deformation. Hot rolling was carried out at 450 °C, during which each rolling pass imposed an approximate thickness reduction of 5%, resulting in a total deformation of 45%. Immediately after the final rolling pass, the samples were quenched in water to retain the deformed microstructure. Subsequently, a stress-relief annealing treatment was performed at 400 °C for 6 h to alleviate residual stresses introduced during the rolling process and to promote microstructural stabilization. Meanwhile, the as-cast ingots were first subjected to a homogenization treatment at 400 °C for 2 h, followed by water quenching. This temperature was selected as it is sufficiently high to promote diffusion of alloying elements (Ca and Ag) and partial dissolution/redistribution of the eutectic Mg_2Ca phase, thereby reducing compositional segregation without approaching the eutectic temperature (~517 °C in the Mg-Ca binary system) that could cause incipient melting. Subsequently, after multi-pass hot rolling, a stress-relief annealing was performed at the same temperature of 400 °C but for a longer duration of 6 h. The identical temperature ensures process consistency and microstructural stability, while the extended holding time facilitates effective recovery (dislocation rearrangement and annihilation) and alleviation of rolling-induced residual stresses without triggering excessive recrystallization or significant grain coarsening, which is critical for retaining the deformation texture and precipitation potential in the Mg-Ca-Ag system. This parameter selection is commonly adopted in Mg-Ca-based alloys to balance homogenization efficiency, stress relief, and avoidance of undesirable phase transformations or over-aging. Microstructural characterization was conducted using scanning electron microscopy (SEM) (ZEISS Sigma 500, Oberkochen, Germany) equipped with an energy-dispersive X-ray spectroscopy (EDS) (ZEISS Sigma 500, Oberkochen, Germany) system, operating at an accelerating voltage of 15 kV. Transmission electron microscopy (TEM) (FEI Helios NanoLab, Hillsboro, OR, USA) specimens were prepared by mechanical grinding followed by focused ion beam (FIB) milling to obtain electron-transparent foils suitable for high-resolution observation. The corrosion behavior of the alloy was evaluated by immersion tests conducted in simulated body fluid (SBF) under static conditions. The specimens were immersed for a duration of 3 h, during which hydrogen evolution was continuously monitored and recorded at 10 min intervals to quantify the corrosion kinetics. After immersion, the surface morphology and three-dimensional surface profiles of the corroded specimens were examined using SEM and optical profilometry(Bruker ContourGT, Billerica, MA, USA), enabling a detailed assessment of corrosion characteristics and pit morphology.

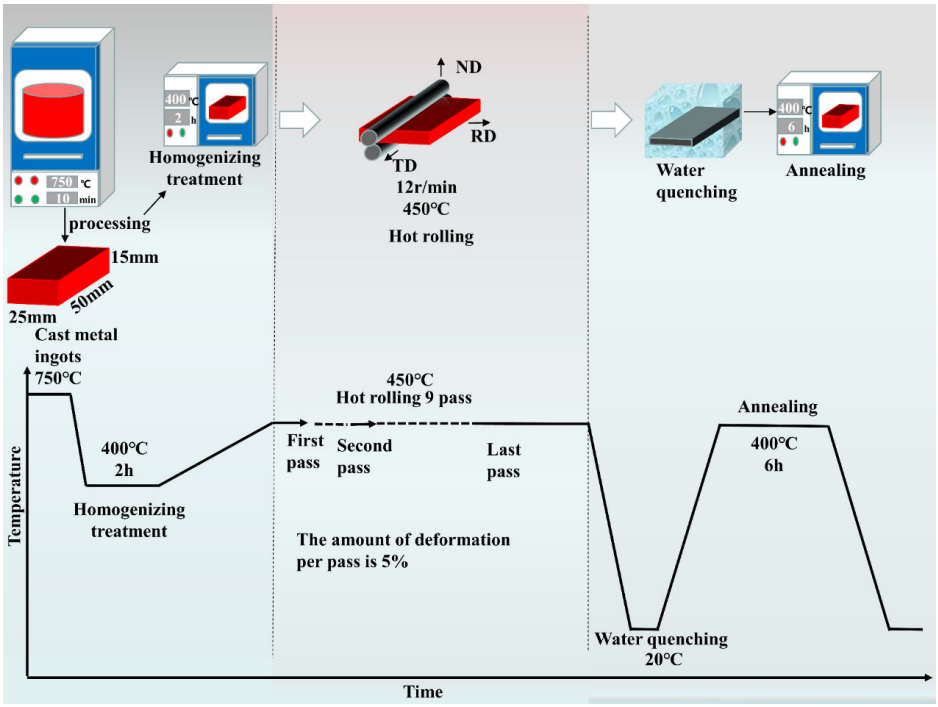


Figure 1. Schematic diagram of the magnesium alloy preparation process.

3. Results and Discussion

Figure 2 illustrates the effect of Ag addition on the microstructural evolution of the Mg-1Ca alloy in both the as-cast and hot-rolled conditions. In the as-cast state, the microstructure of the Mg-1Ca alloy is composed primarily of an α-Mg matrix accompanied by a continuous, network-like distribution of coarse secondary precipitates. Upon the addition of Ag, the overall phase constitution remains essentially unchanged; however, a noticeable refinement in grain size can be observed, as shown in Figure 2a,c. This indicates that Ag addition slightly suppresses grain growth during solidification without introducing new phases. X-ray diffraction (XRD) phase analysis, as presented in Figure 2i, further confirms that the matrix phase in both alloys is α-Mg, while the network-distributed coarse precipitates are identified as Mg_2Ca. These results are consistent with those reported in previous studies [22], confirming that Ag does not alter the primary phase formation behavior in the as-cast Mg–Ca system. After hot rolling, significant changes in deformation microstructures are observed. In the hot-rolled Mg-1Ca alloy, a large number of elongated {10–12} tensile twins are generated, as shown in Figure 2e, indicating that tensile twinning serves as the dominant deformation mechanism under the applied rolling conditions. In contrast, the hot-rolled Mg-1Ca-2Ag alloy exhibits not only tensile twins but also a considerable fraction of thicker double twins, as illustrated in Figure 2g. This suggests that Ag addition markedly influences the activation of twinning modes during plastic deformation. More importantly, a high density of fine nanoscale precipitates is observed in the vicinity of twin boundaries in the Mg-1Ca-2Ag alloy after rolling (Figure 2h). The preferential formation of these nanoscale phases near twin interfaces implies that twin boundaries act as effective nucleation sites for precipitate formation. This phenomenon can be attributed to the combined effects of Ag addition and thermomechanical deformation, which promote localized solute segregation and dynamic precipitation, as further evidenced in Figure 2b,d,f. To quantitatively assess the influence of Ag on the twinning behavior during hot rolling, electron backscatter diffraction (EBSD) analysis was conducted, as shown in Figure 2j–m. The EBSD results clearly reveal that Ag addition significantly alters the twinning characteristics. Specifically, the area fraction of tensile twins decreases sharply

from 42.7% in the Mg-1Ca alloy to 11.5% in the Mg-1Ca-2Ag alloy, whereas the fraction of double twins increases dramatically from 1.02% to 19.2%. The combined effects of increased crystallographic orientation variation and the presence of nanoscale Ag_3Mg particles along internal twin boundaries give rise to localized stress concentrations around the {10–12} twin interfaces. These internal stresses provide the driving force for further reorientation, facilitating the nucleation of secondary {10–12} twins on different variants and ultimately triggering the formation of {10–12}–{10–12} double twins. The characteristic lattice reorientation associated with each {10–12} tensile twinning event is approximately 86° (precisely 86.3° for Mg). This value can be geometrically determined as follows: In hcp magnesium, the {10–12} twinning plane forms an angle of approximately 43.15° with the basal (0001) plane. Since {10–12} twinning approximates a mirror reflection across the twinning plane (with minor adjustments due to atomic shuffles required to restore the lattice), the c-axis in the twinned region is reoriented by approximately twice this dihedral angle, i.e., ~86.3°, relative to the parent c-axis. The precise angle is calculated based on the c/a ratio of Mg (1.6236), yielding a misorientation of 86.3° about the <11–20> axis. This substantial reorientation places the primary twin in a crystallographically favorable position for secondary twinning under continued deformation and local stress accumulation induced by the pinning effect of Ag_3Mg nanoparticles. Correspondingly, this shift in twinning mode leads to pronounced changes in crystallographic orientation and texture evolution. The texture intensity decreases from 2.36 to 2.04 after Ag addition, indicating that Ag slightly weakens the basal texture of the hot-rolled Mg-1Ca alloy. Such texture weakening is expected to influence both mechanical anisotropy and subsequent corrosion behavior, thereby playing a critical role in the overall performance of the alloy.

Based on the field emission scanning electron microscopy (FESEM) observations shown in Figure 2g, and further corroborated by transmission electron microscopy (TEM) analysis, the phase composition of the nanoscale precipitates distributed near twin boundaries in the hot-rolled Mg-1Ca-2Ag alloy was systematically investigated. As illustrated in the TEM bright-field image in Figure 3a, a large number of particle-like nanoscale precipitates can be clearly observed in close proximity to the twin boundaries, indicating a strong spatial correlation between twin interfaces and precipitate formation. Energy-dispersive X-ray spectroscopy (EDS) elemental mapping results, presented in Figure 3c–e, reveal that these nanoscale precipitates are predominantly enriched in Ag and Mg, while no significant Ca enrichment is detected. This elemental distribution suggests that the precipitates are Ag–Mg-based intermetallic compounds rather than Ca-containing phases. To further identify the crystal structure of these nanoprecipitates, high-resolution TEM (HRTEM) images were analyzed using fast Fourier transform (FFT) techniques with Digital Micrograph (DM) software (DM3.0), as shown in Figure 3f,g. Silver exhibits limited solid solubility in solid magnesium. According to the assessed Mg-Ag binary phase diagram, the maximum solid solubility of Ag in α-Mg is approximately 15.5 wt.% at the eutectic temperature of 472 °C, but decreases sharply to nearly negligible values at lower temperatures [26,27]. Given the low Ag content (2 wt.%) in the present alloy, which is well below the maximum solubility at elevated temperatures, no additional Ag-containing phases were detected by XRD in the as-cast condition, indicating that Ag is primarily retained in solid solution or forms precipitates below the XRD detection limit. However, during hot rolling, the high thermal diffusivity of Ag promotes its segregation to deformation-induced twin boundaries, leading to dynamic precipitation of nanoscale Ag_3Mg intermetallic particles, as confirmed by TEM and HRTEM (Figure 3). Although various intermetallic compounds (e.g., Ag_3Mg, Mg_4Ag, Mg_3Ag, MgAg, $AgMg_3$) have been reported in the Mg-Ag system [28–31], the precipitates observed here under the specific low-Ag and thermomechanical conditions are unambiguously identified as the Ag_3Mg phase, with an interplanar spacing of ~0.110 nm

corresponding to the (318) plane. This result confirms that the nanoscale precipitates formed near the twin boundaries are Ag_3Mg intermetallic compounds. The formation mechanism of the Ag_3Mg phase can be primarily attributed to the substantially higher thermal diffusion coefficient of Ag atoms relative to Ca atoms in the α-Mg matrix [32]. During the hot rolling process, {10–12} tensile twins are first activated and generated within the grains, as shown in Figure 2e,g. According to previous studies [21], twin boundaries act as effective barriers to long-range solute diffusion. Consequently, Ag atoms migrating during hot deformation tend to accumulate preferentially near these twin boundaries. The localized enrichment of Ag, combined with the elevated temperature and strain-induced defects during hot rolling, provides favorable thermodynamic and kinetic conditions for the nucleation and growth of Ag_3Mg nanoparticles. As a result, finely dispersed Ag_3Mg precipitates form preferentially along twin boundaries, as schematically and experimentally evidenced in Figure 3a.

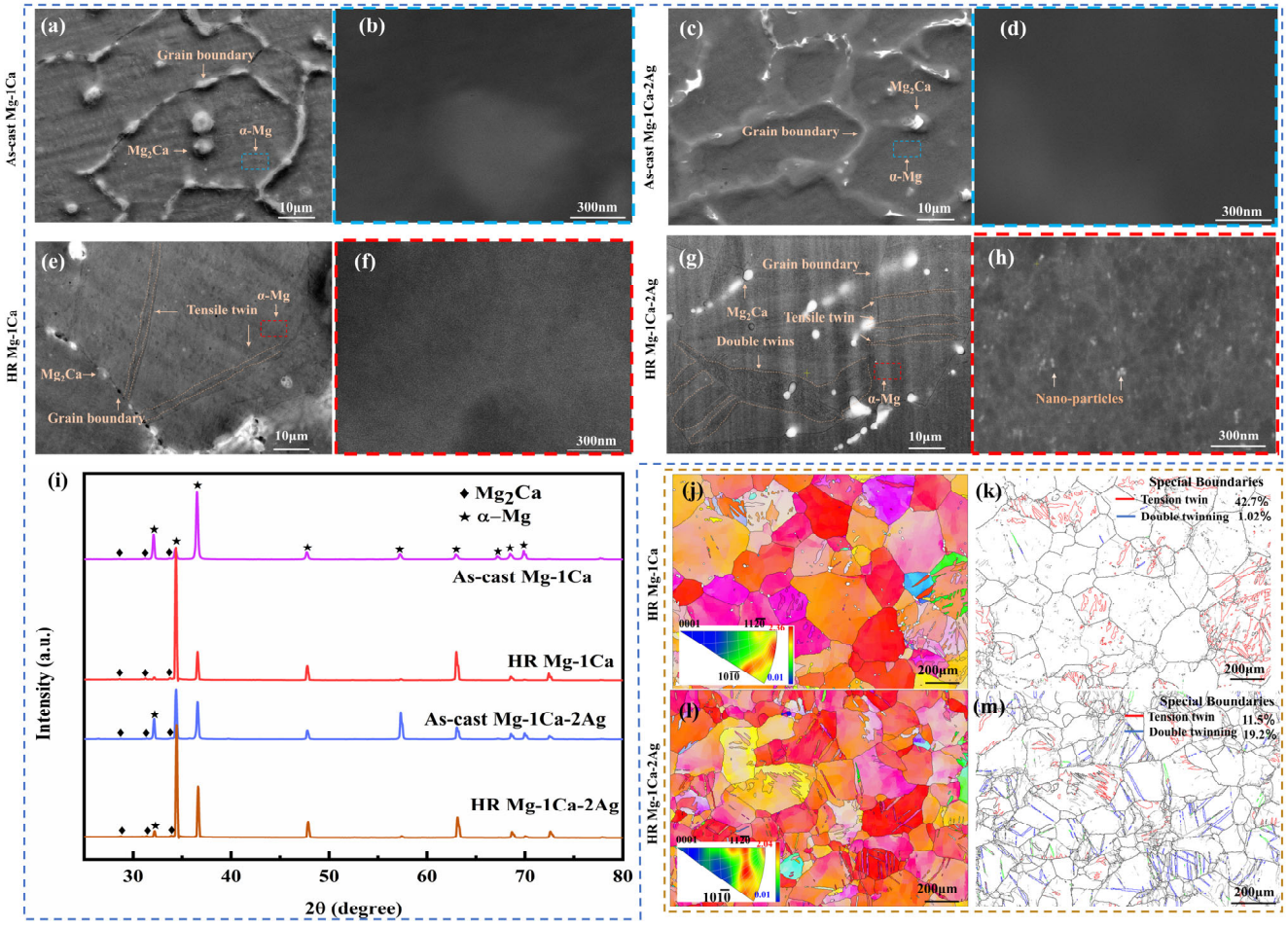


Figure 2. (**a**,**b**) FESEM images of as-cast Mg-1Ca alloy; (**c**,**d**) FESEM images of as-cast Mg-1Ca-2Ag alloy; (**e**,**f**) FESEM images of hot-rolled Mg-1Ca alloy; (**g**,**h**) FESEM images of hot-rolled Mg-1Ca-2Ag alloy; (**i**) XRD spectra of Mg-1Ca and Mg-1Ca-2Ag alloys; (**j**,**k**) Grain orientation maps and twin type distribution of hot-rolled Mg-1Ca alloy; (**l**,**m**) Grain orientation maps and twin type distribution of hot-rolled Mg-1Ca-2Ag alloy.

The formation of Ag_3Mg nanoparticles in the vicinity of {10–12} tensile twin boundaries plays a critical role in promoting the transformation of tensile twins into double twins during subsequent plastic deformation, as schematically illustrated in Figure 4. Specifically, the precipitation of Ag_3Mg nanoparticles near twin boundaries effectively impedes boundary migration by exerting a pinning effect, thereby restricting the growth and stability

of pre-existing tensile twins. As plastic deformation progresses, grain rotation becomes increasingly pronounced, facilitating the formation of a high density of high-angle grain boundaries. This process enhances crystallographic orientation diversity within the microstructure and leads to a gradual reduction in texture intensity, as evidenced by the EBSD results shown in Figure 2j,l. The weakened basal texture reflects a more randomized orientation distribution, which is closely associated with the altered deformation mechanisms induced by Ag addition. Furthermore, the combined effects of increased crystallographic orientation variation and the presence of nanoscale Ag_3Mg particles along internal twin boundaries give rise to localized stress concentrations around the {10–12} twin interfaces. These internal stresses provide the driving force for the reorientation of tensile twins. As a result, the {10–12} tensile twins undergo a rotation of approximately 86° about the grain c-axis, ultimately triggering the formation of {10–12}–{10–12} double twins, in accordance with the crystallographic characteristics of double twinning in Mg alloys [33]. This twinning transformation mechanism provides a clear explanation for the distinct differences in twin distribution observed between the two alloys. As shown in Figure 2k,m, the hot-rolled Mg-1Ca alloy is dominated by a high fraction of tensile twins and contains only a limited number of double twins. In contrast, the hot-rolled Mg-1Ca-2Ag alloy exhibits a significantly reduced tensile twin fraction accompanied by a markedly increased population of double twins. These observations confirm that the synergistic effects of Ag addition and Ag_3Mg nanoprecipitation fundamentally modify the twinning behavior and deformation pathways of the Mg–Ca alloy during hot rolling.

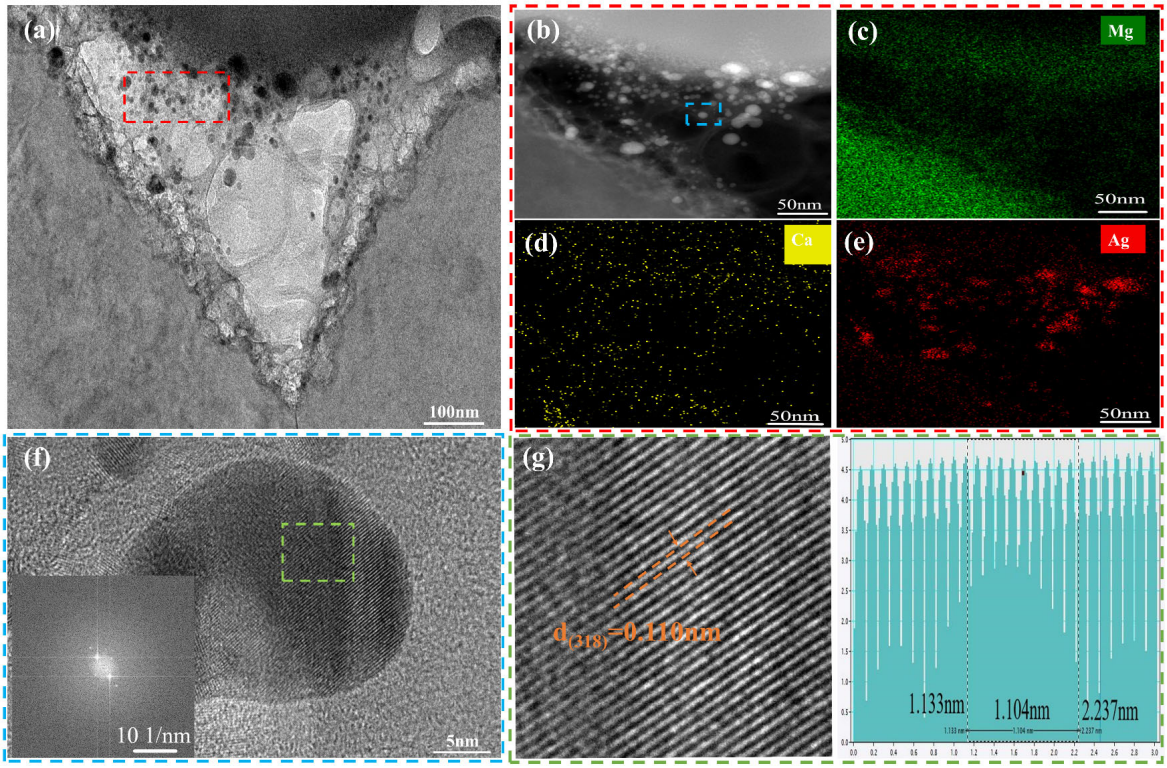


Figure 3. Phase distribution and TEM analysis of hot-rolled Mg-1Ca-2Ag alloy: (**a**) Twins and nanoscale precipitates in hot-rolled Mg-1Ca-2Ag; (**b**–**e**) TEM images and EDS elemental maps of nanoscale precipitates; (**f**,**g**) Lattice spacing of nanoscale particles.

The influence of Ag_3Mg nanoparticles and double twins, formed during the hot rolling process, on the corrosion behavior of the alloys is illustrated in Figure 5h,j. First, the hot-rolled Mg-1Ca alloy exhibits a markedly higher hydrogen evolution rate when immersed in simulated body fluid (SBF), indicating a significantly faster corrosion rate compared to that

of the hot-rolled Mg-1Ca-2Ag alloy, as shown in Figure 5g. This result clearly demonstrates that Ag addition effectively suppresses the corrosion kinetics of the Mg–Ca alloy system. Second, analysis of the surface corrosion morphology, as shown in Figure 5a–f, reveals substantial differences in corrosion characteristics between the two alloys. For the hot-rolled Mg-1Ca alloy, the corrosion products are distributed in a highly non-uniform manner across the surface (Figure 5a). Severe localized corrosion is observed, accompanied by the formation of deep corrosion pits with depths exceeding 80 μm (Figure 5c). Such localized pitting corrosion is detrimental to the structural integrity of biodegradable implants, as it can lead to premature mechanical failure. In contrast, the hot-rolled Mg-1Ca-2Ag alloy exhibits significantly enhanced corrosion resistance. The presence of {10–12} double twins promotes a more homogeneous microstructural configuration with increased grain boundary density, which facilitates the formation of a more uniform and continuous corrosion product layer on the alloy surface (Figure 5d). This uniform corrosion behavior effectively mitigates localized corrosion attack. More importantly, during the corrosion process, the corrosion product film formed in the vicinity of Ag_3Mg nanoparticles plays a crucial role in inhibiting the vertical propagation of corrosion pits. The locally dense and adherent corrosion product layer surrounding the Ag_3Mg precipitates acts as a physical barrier, limiting the penetration of corrosive media into the matrix. As a result, the maximum corrosion pit depth in the Mg-1Ca-2Ag alloy is reduced to approximately 35 μm (Figure 5f), which is less than half of that observed in the Ag-free alloy. In summary, the introduction of Ag into the Mg-1Ca alloy promotes the formation of double twins during hot rolling, leading to an increased density of grain and twin boundaries and, consequently, enhanced corrosion uniformity. Simultaneously, the presence of Ag_3Mg nanoparticles contributes to the formation of a more protective corrosion product film that effectively suppresses localized pitting corrosion. In addition, the introduction of noble metal elements (e.g., Ag) into Mg alloys leads to the formation of secondary phases (such as Ag_3Mg or $Mg_{54}Ag_{17}$) with an electrochemical potential higher than that of the α-Mg matrix. Theoretically, this can establish a galvanic couple, where Ag-containing nanoprecipitates act as cathodes, promoting accelerated dissolution of the Mg matrix and potentially influencing the corrosion rate and localized corrosion tendency. However, the intensity of the electrochemical effect is highly dependent on the size, distribution, and volume fraction of the secondary phases. When the secondary phases exist as highly dispersed nanoparticles, the cathode area is significantly smaller than the anode area. This results in a substantial reduction in the electrochemical current density, leading to only a weak acceleration effect. Conversely, fine particles tend to promote a more uniform distribution of corrosion, avoiding the severe localized pitting often induced by coarse secondary phases. Furthermore, Ag may undergo re-deposition or dealloying during corrosion, releasing Ag^+ ions that provide antibacterial activity without significantly compromising the overall degradation profile. In this study, the design of Ag_3Mg nanoparticles aims to leverage their potential for strengthening and functional benefits while minimizing the negative impact of the electrochemical effect through nanoscale control. The uniform corrosion morphology and the formation of a protective Ca-P/$Mg(OH)_2$ layer observed in immersion tests indicate that the electrochemical effect did not lead to adverse localized acceleration [34,35]. The synergistic effects of microstructural refinement, twin-induced texture modification, and nanoprecipitate-assisted corrosion inhibition collectively result in a significant improvement in the overall corrosion resistance of the Mg-1Ca-Ag alloy system [23].

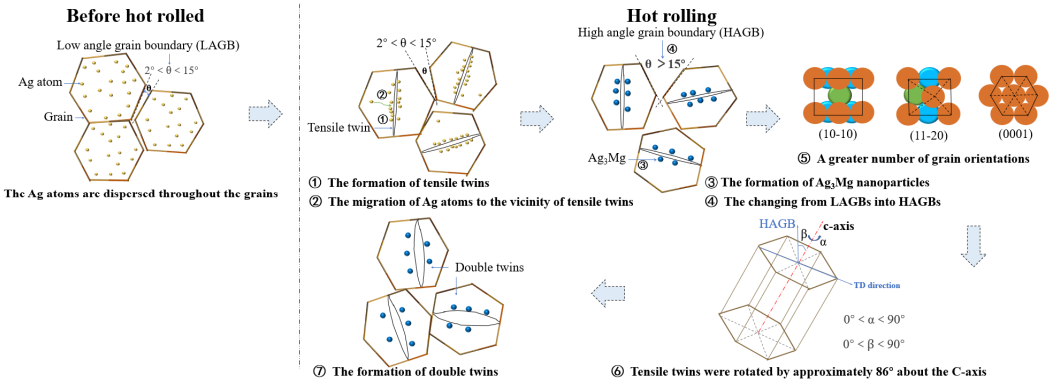


Figure 4. Schematic diagram of the effect of Ag_3Mg nanoscale particles on twin formation and grain orientation evolution during deformation in hot-rolled Mg-1Ca-2Ag.

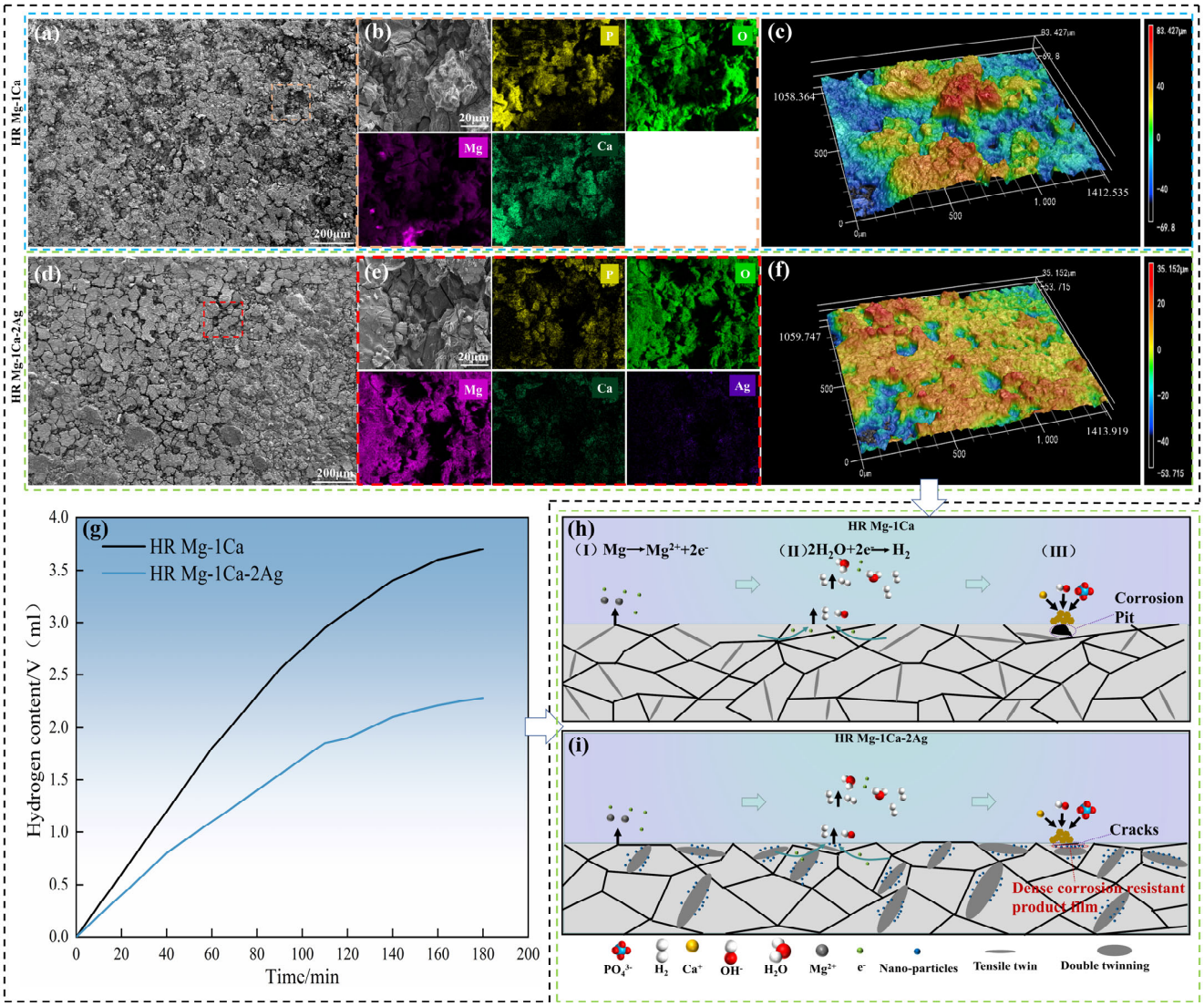


Figure 5. Morphological characterization of alloys after 3 h immersion in simulated body fluid (SBF): (**a**) SEM micrograph showing corrosion morphology of HR Mg-1Ca alloy; (**b**) EDS elemental mapping of HR Mg-1Ca alloy; (**c**) 3D topographic profile of corroded HR Mg-1Ca alloy surface; (**d**) SEM micrograph of corroded HR Mg-1Ca-2Ag alloy; (**e**) EDS elemental mapping of HR Mg-1Ca-2Ag alloy; (**f**) 3D surface topography of corroded HR Mg-1Ca-2Ag alloy; (**g**) Corrosion rate comparison between HR Mg-1Ca and HR Mg-1Ca-2Ag alloys; (**h**) Schematic representation of corrosion mechanism in HR Mg-1Ca alloy; (**i**) Schematic representation of corrosion mechanism in HR Mg-1Ca-2Ag alloy.

4. Conclusions

In this study, the introduction of Ag into a Mg-1Ca alloy and its subsequent plastic deformation via hot rolling were employed to systematically investigate the microstructural evolution and corrosion behavior of the alloy. Based on experimental results, the following conclusions were drawn: Firstly, upon the addition of Ag, the as-cast microstructure of the alloy remained consistent with the Mg-1Ca alloy, comprising Mg_2Ca and α-Mg phases. Secondly, during the hot rolling process, the relatively high thermal diffusivity of Ag atoms led to their enrichment at the tensile twin boundaries, where they combined with Mg to form Ag_3Mg nanoparticles. The precipitation of Ag_3Mg nanoparticles near the twin boundaries inhibited grain boundary migration. As deformation progressed, grain rotation facilitated the formation of a significant number of high-angle grain boundaries, which resulted in an increase in the crystallographic orientations and a reduction in texture strength. Furthermore, the increased number of grain orientations, combined with the presence of nanoparticles near the twin boundaries, induced internal stresses, which caused the {10–12} tensile twins to rotate approximately 86° around the c-axis, ultimately leading to the formation of double twins. Finally, during corrosion, the synergistic effect of the nanoparticles and double twins facilitated the formation of a dense protective film, effectively reducing the corrosion rate and enhancing the overall corrosion resistance of the alloy.

Author Contributions: Z.L.: Conceptualization, Resources, Project Administration, Funding Acquisition, Validation, Formal Analysis. Q.Q.: Conceptualization, Methodology, Software, Data Curation, Writing—Original Draft Preparation, Writing—Review and Editing, Validation. D.S.: Software, Validation. Q.J.: Conceptualization, Data Curation, Formal Analysis, Writing—Original Draft, Visualization, Supervision. Y.S.: Conceptualization, Formal Analysis, Writing—Original Draft, Investigation. All authors have read and agreed to the published version of the manuscript.

Funding: This project was supported by the Guizhou Provincial Department of Education Open Recruitment and Leadership Scientific and Technological Attack Project (Guizhou Education Technology [2024] No. 003), Open Project of Yunnan Precious Metals Laboratory Co., Ltd. (No.YPML-20240502016) Doctoral Fund Project of Anshun University (No.asxybsjj202414) National Natural Science Foundation of China (No.51864026).

Data Availability Statement: The data presented in this study are available on request from the corresponding author.

Conflicts of Interest: Author Daliang Sun was employed by the Baoti Group Co., Ltd. The remaining authors declare that the research was conducted in the absence of any commercial or financial relationships that could be construed as a potential conflict of interest.

References

1. Lahbari, A.; Bouchaala, K.; Essoussi, H.; Faqir, M.; Ettaqi, S.; Essadiqi, E.H. Homogenization Heat Treatment Influence on Microstructure Evolution and Mechanical Properties of As-Cast Al-Li-Cu-Mg-Zr Alloy for Lightweight Aerospace Application. *Heliyon* **2024**, *10*, e24426. [CrossRef]
2. Ling, N.; Wang, Y.; Song, S.; Liu, C.; Yang, F.; Qi, X.; Li, Y.; Zhang, J.; Wang, L. Experimentally Validated Screening Strategy for Alloys As Anode in Mg-air Battery with Multi-Target Machine Learning Predictions. *Chem. Eng. J.* **2024**, *496*, 153824. [CrossRef]
3. Ji, C.; Ma, A.; Jiang, J.; Song, D.; Liu, H.; Guo, S. Research status and future prospects of biodegradable Zn-Mg alloys. *J. Alloys Compd.* **2024**, *993*, 174669. [CrossRef]
4. Chen, J.; Tan, L.; Yu, X.; Etim, I.P.; Ibrahim, M.; Yang, K. Mechanical properties of magnesium alloys for medical application: A review. *J. Mech. Behav. Biomed. Mater.* **2018**, *87*, 68–79. [CrossRef]
5. Zander, D.; Zumdick, N.A. Influence of Ca and Zn on the Microstructure and Corrosion of Biodegradable Mg–Ca–Zn Alloys. *Corros. Sci.* **2015**, *93*, 222–233. [CrossRef]

6. Kirkland, N.T.; Birbilis, N.; Walker, J.; Woodfield, T.; Dies, G.J.; Steiger, M.P. In-vitro Dissolution of Magnesium-Calcium Binary Alloys: Clarifying the Unique Role of Calcium Additions in Bioresorbable Magnesium Implant Alloys. *J. Biomed. Mater. Res. Part B Appl. Biomater.* **2010**, *95*, 91–100. [CrossRef] [PubMed]
7. Chen, H.; Yuan, B.; Zhao, R.; Yang, X.; Xiao, Z.; Aurora, A.; Iulia, B.A.; Zhu, X.; Iulian, A.V.; Zhang, X. Evaluation on the Corrosion Resistance, Antibacterial Property and Osteogenic Activity of Biodegradable Mg-Ca and Mg-Ca-Zn-Ag Alloys. *J. Magnes. Alloys* **2022**, *10*, 3380–3396. [CrossRef]
8. Wang, X.; Luo, T.; Zheng, C.; Li, Y.; Huang, Q.; Yang, Y. Microstructure Evolution and Dynamic Recrystallization Mechanisms of Mg-Al-Ca-Zn-Sn-Mn Alloys with Different Ca Contents During Hot Extrusion. *J. Alloys Compd.* **2025**, *1011*, 178400. [CrossRef]
9. Shangguan, F.-E.; Cheng, W.-L.; Chen, Y.-H.; Cui, Z.-Q.; Yu, H.; Wang, H.-X.; Wang, L.-F.; Li, H.; Hou, H. Role of Micro-Ca/in Alloying in Tailoring the Microstructural Characteristics and Discharge Performance of Dilute Mg-Bi-Sn-based Alloys As Anodes for Mg-air Batteries. *J. Magnes. Alloys* **2024**, *12*, 251–266. [CrossRef]
10. Cheng, W.; Hao, X.; Shangguan, F.; Chen, Y.; Yu, H.; Wang, L.; Cui, Z.; Li, H.; Zhang, X.; Wang, J.; et al. Electrochemical Behavior and Discharge Performance of Dilute Mg-Bi-Based Alloy As an Anode for Primary Mg-Air Battery. *Mater. Charact.* **2024**, *209*, 113688. [CrossRef]
11. Minarik, P.; Kral, R.; Cizek, J.; Chmelik, F. Effect of Different C/A Ratio on the Microstructure and Mechanical Properties in Magnesium Alloys Processed by Ecap. *Acta Mater.* **2016**, *107*, 83–95. [CrossRef]
12. Bian, M.; Huang, X.; Chino, Y. A Combined Experimental and Numerical Study on Room Temperature Formable Magnesium–silver–calcium Alloys. *J. Alloys Compd.* **2020**, *834*, 155017. [CrossRef]
13. Zhang, X.; Ba, Z.; Wang, Z.; He, X.; Shen, C.; Wang, Q. Influence of Silver Addition on Microstructure and Corrosion Behavior of Mg–Nd–Zn–Zr Alloys for Biomedical Application. *Mater. Lett.* **2013**, *100*, 188–191. [CrossRef]
14. Ouyang, S.; Wu, X.; Meng, L.; Jing, X.; Qiao, L.; She, J.; Zheng, K.; Chen, X.; Pan, F. More Than the Barrier Effect: Biodegradable Mg-Ag Alloy Membranes for Guided Bone/tissue Regeneration. *J. Magnes. Alloys* **2024**, *12*, 4454–4467. [CrossRef]
15. Cheng, R.; Zhou, Y.; Wang, H.; Jiang, L.; Tang, A.; Jiang, B. Influence of Ag on the Precipitates in Mg-8Gd-0.8Y-0.5Zn-0.3Zr Alloy. *J. Mater. Res. Technol.* **2025**, *34*, 577–584.
16. Shangguan, F.-E.; Cheng, W.-L.; Chen, Y.-H.; Yu, H.; Wang, L.-F.; Li, H.; Wang, H.-X.; Wang, J.-H. Elucidating the Dependence of Electrochemical Behavior and Discharge Performance on the Grain Structure of Lean Mg-0.3bi-0.3ag-0.3in Anodes in Primary Mg-Air Battery. *J. Power Sources* **2022**, *564*, 232856. [CrossRef]
17. Yang, S.L.; Wilson, N.; Esser, B.D.; Etheridge, J.; Nie, J.F. Distribution of Ag and Mg in T1 Precipitate Plates in an Al-Cu-Li-Mg-Ag Alloy. *Acta Mater.* **2025**, *286*, 120763. [CrossRef]
18. Weng, Y.; Ding, L.; Zhang, Z.; Jia, Z.; Wen, B.; Liu, Y.; Muraishi, S.; Li, Y.; Liu, Q. Effect of Ag Addition on the Precipitation Evolution and Interfacial Segregation for Al–Mg–Si Alloy. *Acta Mater.* **2019**, *180*, 301–316. [CrossRef]
19. Macchi, C.; Tolley, A.; Giovachini, R.; Polmear, I.J.; Somoza, A. Influence of a Microalloying Addition of Ag on the Precipitation Kinetics of an Al–Cu–Mg Alloy with High Mg:Cu Ratio. *Acta Mater.* **2015**, *98*, 275–287. [CrossRef]
20. Kannan, M.B.; Singh Raman, R.K. In Vitro Degradation and Mechanical Integrity of Calcium-Containing Magnesium Alloys in Modified-Simulated Body Fluid. *Biomaterials* **2008**, *29*, 2306–2314. [CrossRef]
21. Yan, H.; Shao, X.H.; Li, H.P.; Chen, R.S.; Cui, H.Z.; Han, E.H. Synergization of Ductility and Yield Strength in a Dilute Quaternary Mg-Zn-Gd-Ca Alloy Through Texture Modification and Guinier–Preston Zone. *Scr. Mater.* **2021**, *207*, 114257. [CrossRef]
22. Martynenko, N.; Anisimova, N.; Rybalchenko, G.; Lukyanova, E.; Rybalchenko, O.; Shchetinin, I.; Babayeva, G.; Pashinzeva, N.V.; Gorbenko, A.; Temralieva, D.; et al. Effect of warm rotary swaging on the mechanical and operational properties of the biodegradable Mg-1%Zn-0.6%Ca alloy. *J. Magnes. Alloys* **2025**, *13*, 2252–2266. [CrossRef]
23. Tao, M.; Cui, Y.; Sun, S.; Zhang, Y.; Ge, J.; Yin, W.; Li, P.; Wang, Y. Versatile Application of Magnesium-Related Bone Implants in the Treatment of Bone Defects. *Mater. Today Bio* **2025**, *31*, 101635. [CrossRef]
24. Li, W.; Huang, X.; Huang, W. Effects of Ca, Ag Addition on the Microstructure and Age-Hardening Behavior of a Mg-7Sn (wt%) Alloy. *Mater. Sci. Eng. A* **2017**, *692*, 75–80. [CrossRef]
25. Koike, J. Enhanced Deformation Mechanisms by Anisotropic Plasticity in Polycrystalline Mg Alloys at Room Temperature. *Metall. Mater. Trans. A* **2005**, *36*, 1689–1696. [CrossRef]
26. Lim, M.; Tibballs, J.E.; Rossiter, P.L. Thermodynamic Assessment of the Ag–Mg Binary System. *Int. J. Mater. Res.* **1997**, *88*, 162–169.
27. Nayeb-Hashemi, A.A.; Clark, J.B. The Ag-Mg (Silver-Magnesium) system. *Bull. Alloy Phase Diagr.* **1988**, *9*, 468–473. [CrossRef]
28. Cao, W.; Ding, X.; Zhang, Y.; Zhang, J.; Chen, R.; Su, Y.; Guo, J.; Fu, H. Enhanced de-/hydrogenation kinetics of a hyper-eutectic $Mg_{85}Ni_{15-x}Ag_x$ alloy facilitated by Ag dissolving in Mg_2Ni. *J. Alloys Compd.* **2022**, *917*, 165457. [CrossRef]
29. Terlicka, S.; Dębski, A.; Sypień, A.; Gąsior, W.; Budziak, A. Determination of thermophysical and thermodynamic properties of Ag-Mg alloys. *Mater. Today Commun.* **2021**, *29*, 102946. [CrossRef]
30. Pęska, M.; Smektalska, K.; Dworecka-Wójcik, J.; Terlicka, S.; Gąsior, W.; Gierlotka, W.; Dębski, A.; Polański, M. Hydrogen sorption behavior of mechanically synthesized Mg–Ag alloys. *Int. J. Hydrogen Energy* **2021**, *46*, 33152–33163. [CrossRef]

31. Yang, L.; Shi, Y.; Shen, L.; Zhang, E.; Qin, G.; Lu, X.; Zhou, X. Effect of Ag on cathodic activation and corrosion behaviour of Mg-Mn-Ag alloys. *Corros. Sci.* **2021**, *185*, 109408. [CrossRef]
32. Stloukal, I.; Cermak, J. Silver Diffusion in Commercial QE22 Magnesium Alloy with Saffil Fiber Reinforcement. *Compos. Sci. Technol.* **2008**, *68*, 2799–2803. [CrossRef]
33. Hu, X.; Ji, Y.; Chen, L.; Lebensohn, R.A.; Chen, L.Q.; Cui, X. Spectral phase-field model of deformation twinning and plastic deformation. *Int. J. Plast.* **2021**, *143*, 103019. [CrossRef]
34. Xu, L.; Liu, X.; Sun, K.; Fu, R.; Wang, G. Corrosion Behavior in Magnesium-Based Alloys for Biomedical Applications. *Materials* **2022**, *15*, 2613. [CrossRef] [PubMed]
35. Kubásek, J.; Minárik, P.; Vosmanská, K.; Čapek, J.; Drahokoupil, J.; Vojtěch, D. Microstructure and Corrosion Behaviour of Mg-Ca and Mg-Zn-Ag Degradable Alloys. *Crystals* **2023**, *13*, 1213. [CrossRef]

Disclaimer/Publisher's Note: The statements, opinions and data contained in all publications are solely those of the individual author(s) and contributor(s) and not of MDPI and/or the editor(s). MDPI and/or the editor(s) disclaim responsibility for any injury to people or property resulting from any ideas, methods, instructions or products referred to in the content.